

Cite this: *Chem. Sci.*, 2025, 16, 9756

All publication charges for this article have been paid for by the Royal Society of Chemistry

# Self-promoted tumor-targeting nanomedicine activates STING-driven antitumor immunity via photodynamic DNA damage and PARP inhibition†

Baixue Yu,<sup>‡a</sup> Wei Zhang,<sup>‡a</sup> Zhouchuan Shao,<sup>a</sup> Xiayun Chen,<sup>a</sup> Yi Cen,<sup>a</sup> Yibin Liu,<sup>a</sup> Ying Chen,<sup>a</sup> Xinxuan Li,<sup>a</sup> Ziqi Liang,<sup>a</sup> Shiyang Li<sup>ID</sup>\*<sup>ab</sup> and Xiaoyuan Chen<sup>ID</sup>\*<sup>bcdefghi</sup>

The activation of antitumor immunity through strategically designed nanomedicine presents a promising approach to overcome the limitations of conventional cancer therapies. In this work, bioinformatic analysis found an abnormal poly(ADP-ribose) polymerase-1 (PARP-1) expression in breast cancer, linked to the cyclic GMP-AMP synthase (cGAS)-stimulator of the interferon gene (STING) pathway and immune suppression. PARP-1 inhibitor screening revealed olaparib (Ola) as a promising candidate, enhancing DNA damage and potentiating the immunotherapeutic response. Consequently, a self-promoted tumor-targeting nanomedicine (designated as PN-Ola) was proposed to activate STING-driven antitumor immunity through photodynamic DNA damage and PARP inhibition. PN-Ola was composed of a programmed death-ligand 1 (PD-L1) targeting amphiphilic peptide-photosensitizer conjugate (C<sub>16</sub>-K(PpIX)-WHRSYTWNLNT), which effectively encapsulates Ola. Notably, PN-Ola demonstrated selective accumulation in tumor cells that overexpress PD-L1, while concurrently enhancing PD-L1 expression, thereby establishing a self-promoting mechanism for improved drug accumulation within tumor cells. Meanwhile, the photodynamic therapy (PDT) effects of PN-Ola would result in oxidative DNA damage and subsequent accumulation of DNA fragments. Additionally, the PARP inhibition provided by PN-Ola disrupted the DNA repair pathways in tumor cells, leading to a boosted release of DNA fragments that further stimulated STING-driven antitumor immunity. The synergistic mechanism of PN-Ola effectively activates the immunotherapeutic response by enhancing T cell activation and infiltration, leading to the eradication of metastatic tumors without inducing side effects. This study presents a promising strategy to overcome targeting ligand heterogeneity while activating systemic antitumor immunity for the effective eradication of metastatic tumors.

Received 12th March 2025

Accepted 12th April 2025

DOI: 10.1039/d5sc01953b

rsc.li/chemical-science

## Introduction

The activation of antitumor immunity has garnered significant interest in the realm of cancer immunotherapy, as it seeks to harness the immune cells to recognize and eradicate malignant cells. A critical mediator in this process is the stimulator of the interferon gene (STING) pathway, a critical sensor of tumor-derived DNA that triggers a cascade of immune responses.<sup>1–3</sup>

Upon activation, STING triggers the release of type I interferons and pro-inflammatory cytokines, facilitating dendritic cell maturation and the subsequent activation of cytotoxic T lymphocytes (CTLs), essential for a robust antitumor immune response.<sup>4,5</sup> Among the various strategies to induce the release of tumor-derived DNA fragments, photodynamic therapy (PDT) has emerged as a particularly attractive option due to its non-invasive nature and precise, on-demand controllability.<sup>6,7</sup> PDT

<sup>a</sup>The Fifth Affiliated Hospital, Guangdong Provincial Key Laboratory of Molecular Target & Clinical Pharmacology, The NMPA and State Key Laboratory of Respiratory Disease, The School of Pharmaceutical Sciences, Guangzhou Medical University, Guangzhou, 511436, P. R. China. E-mail: lisy-sci@gzhmu.edu.cn

<sup>b</sup>Department of Diagnostic Radiology, Yong Loo Lin School of Medicine, National University of Singapore, 119074, Singapore. E-mail: chen.shawn@nus.edu.sg

<sup>c</sup>Department of Chemical and Biomolecular Engineering, College of Design and Engineering, National University of Singapore, 117575, Singapore

<sup>d</sup>Department of Biomedical Engineering, College of Design and Engineering, National University of Singapore, 117575, Singapore

<sup>e</sup>Department of Pharmacy and Pharmaceutical Sciences, Faculty of Science, National University of Singapore, 117544, Singapore

<sup>f</sup>Clinical Imaging Research Centre, Centre for Translational Medicine, Yong Loo Lin School of Medicine, National University of Singapore, 117599, Singapore

<sup>g</sup>Nanomedicine Translational Research Program, Yong Loo Lin School of Medicine, National University of Singapore, 117597, Singapore

<sup>h</sup>Theranostics Center of Excellence (TCE), Yong Loo Lin School of Medicine, National University of Singapore, 138667, Singapore

<sup>i</sup>Institute of Molecular and Cell Biology, Agency for Science, Technology, and Research (A\*STAR), 138673, Singapore

† Electronic supplementary information (ESI) available. See DOI: <https://doi.org/10.1039/d5sc01953b>

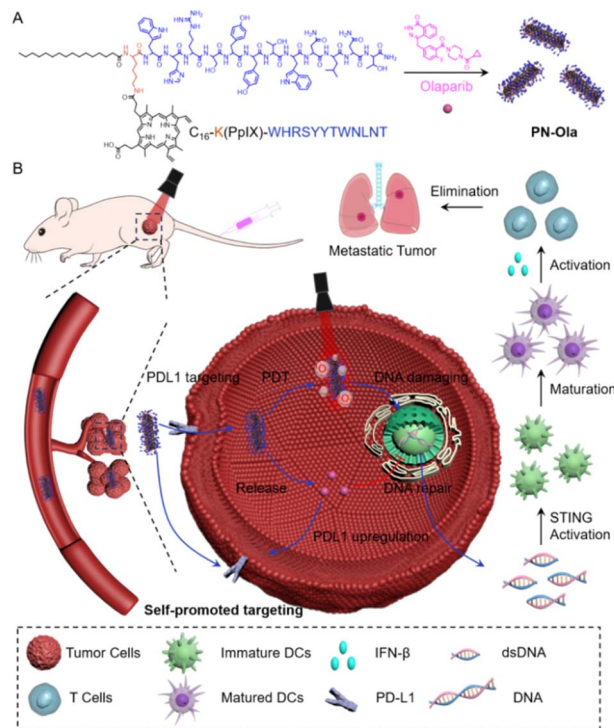
‡ These authors contributed equally to this work.



generates reactive oxygen species (ROS), leading to DNA damage and immunogenic cell death (ICD) in tumor cells.<sup>8–10</sup> However, the effectiveness of PDT is often undermined by the activation of DNA repair pathways within tumor cells, which can mitigate the immunomodulatory effects and limit therapeutic efficacy.<sup>11</sup> To overcome this challenge, the use of poly ADP-ribose polymerase (PARP) inhibitors, known for their role in blocking DNA repair, presents a compelling complementary strategy. By inhibiting PARP, the repair of PDT-induced DNA damage is prevented, leading to increased cellular stress and the amplification of immunogenic signals required for sustained STING pathway activation.<sup>12–14</sup> This synergistic approach not only heightens the susceptibility of tumor cells to PDT but also enhances the overall antitumor immune response, offering a promising avenue for improving the efficacy of photo-immunotherapy.

Despite the potential of combining PDT with PARP inhibition, substantial challenges remain in fully exploiting their immunotherapeutic synergy. Chief among these is the challenge of achieving site-specific co-delivery of both the photosensitizer and PARP inhibitor to enhance synergistic immunomodulation while reducing off-target toxicity.<sup>15</sup> Recent advancements in drug co-delivery systems offer a promising solution, particularly for targeting tumor cells that overexpress programmed death-ligand 1 (PD-L1), a crucial immune checkpoint protein that enables tumors to evade immune detection.<sup>16,17</sup> However, the heterogeneous expression of PD-L1 within and across tumor types presents an essential obstacle, often leading to suboptimal drug delivery and reduced therapeutic efficacy.<sup>18</sup> To address this, there has been growing interest in developing self-promoting drug delivery systems that modulate their targeting receptors, expanding the targeting efficiency and improving overall drug accumulation in tumors.<sup>19,20</sup> Despite these advancements, there are very few reported strategies that actively modulate PD-L1 expression to enhance STING-driven anti-tumor immunity. Such approaches may provide a dual benefit of improving drug delivery efficiency while simultaneously amplifying immune-mediated tumor eradication.

In this study, bioinformatic analysis revealed the abnormal expression of PARP-1 in breast cancer, which was closely linked to the cyclic GMP-AMP synthase (cGAS)-STING signaling pathway and immune suppression. Screening of PARP-1 inhibitors identified olaparib (Ola) as a promising therapeutic candidate, demonstrating its capacity to significantly amplify DNA damage, thereby potentiating the immunotherapeutic response in breast cancer. Based on these mechanistic insights, a self-promoted tumor-targeting nanomedicine (designated as PN-Ola) was fabricated to activate STING-driven antitumor immunity through photodynamic DNA damage and PARP inhibition. Among them, PN-Ola was synthesized by encapsulating PARP inhibitor Ola into a PD-L1 targeting amphiphilic peptide-photosensitizer conjugate of C<sub>16</sub>-K(PpIX)-WHRSYYTWNLNT (Scheme 1A). Benefiting from the targeting peptide sequence, PN-Ola exhibited selective accumulation in tumor cells overexpressing PD-L1. Interestingly, PN-Ola not only targeted these cells but also enhanced PD-L1 expression, creating a self-promoted tumor targeting mechanism for improved drug accumulation. Upon light irradiation,



**Scheme 1** Schematic representation of PN-Ola to activate STING-driven anti-tumor immunity by photodynamic DNA damage and PARP inhibition. (A) Chemical structure of the chimeric peptide and schematic illustration of PN-Ola preparation. (B) PN-Ola demonstrated selective accumulation in tumor cells that overexpress PD-L1, while concurrently enhancing PD-L1 expression, thereby establishing a self-promoting mechanism for improved drug accumulation within tumor cells. Subsequently, the PDT effects of PN-Ola would result in oxidative DNA damage and subsequent accumulation of DNA fragments. Additionally, the PARP inhibition provided by PN-Ola disrupted the DNA repair pathways in tumor cells, leading to a boosted release of DNA fragments that further stimulated STING-driven antitumor immunity. The synergistic effects of PN-Ola could activate the immunotherapeutic response by enhancing T cell activation and infiltration, leading to the eradication of lung metastatic tumors.

PN-Ola produced substantial ROS within tumor cells, resulting in oxidative DNA damage and subsequent accumulation of DNA fragments. Additionally, the PARP inhibition provided by PN-Ola disrupted the DNA repair pathways in tumor cells, leading to the release of DNA fragments that further stimulated STING-mediated antitumor immunity. *In vitro* and *in vivo* assays established that PN-Ola significantly enhanced tumor-targeting drug delivery efficiency while simultaneously activating immunotherapeutic responses, thereby effectively eradicating metastatic tumors through its intricate immune activation mechanism (Scheme 1B).

## Results and discussion

### The close association between PARP-1 overexpression and the cGAS-STING pathway in breast cancer immunity

To elucidate the molecular discrepancies between breast cancer and normal tissues, differentially expressed genes were



systematically analyzed using data from The Cancer Genome Atlas (TCGA). This analysis revealed that PARP-1 was significantly overexpressed compared to normal tissues, suggesting its pivotal role in oncogenesis (Fig. 1A). To further explore their functional interactions, protein interaction networks were constructed using the STRING database. The results evidenced that proteins closely associated with PD-L1 and PARP-1 predominantly converge on the cGAS-STING signaling axis, a pathway critical for DNA damage sensing and immune activation (Fig. 1B). Enrichment analysis through the Kyoto Encyclopedia of Genes and Genomes (KEGG) database provided additional insight, highlighting that PARP-1 is intricately linked to PD-L1 regulation and engages with pathways involving cytoplasmic DNA sensing, JAK-STAT signaling, and T-cell-mediated immunity (Fig. 1C). These findings collectively confirmed the interconnected roles of PD-L1 and PARP-1 in modulating the tumor microenvironment and immune response, laying a foundation for further investigation into their therapeutic potential in breast cancer. Given the critical role of immune cell infiltration in determining the efficacy of immunotherapeutic strategies, the relationship between PARP-1 expression and

immune cell dynamics was further investigated. Interestingly, the analysis displayed a positive correlation between elevated PARP-1 expression and increased infiltration of CD4<sup>+</sup> and CD8<sup>+</sup> T cells, as well as dendritic cells (DCs) (Fig. 1D). However, pharmacological inhibition of PARP-1 is a recognized therapeutic strategy, it might ostensibly hinder immune cell infiltration and compromise antitumor immunity. A plausible explanation lies in the dual role of PARP-1 in DNA damage repair and immune regulation. On one hand, PARP-1 inhibition enhances tumor immunogenicity by preventing DNA repair, leading to cytoplasmic DNA accumulation and subsequent activation of the cGAS-STING pathway. On the other hand, elevated PARP-1 expression facilitated immune cell recruitment *via* the regulation of immunomodulatory pathways. These findings verified that pharmacological modulation of PARP-1 might provide a dual benefit — impairing tumor growth while enhancing antitumor immune responses — making it a promising therapeutic target for breast cancer immunotherapy.

The cGAS-STING pathway is central to anticancer immunity, serving as a critical bridge between innate and adaptive immune responses through the production of type I interferons (IFNs).<sup>21,22</sup> Given the dual roles of PARP-1 in DNA repair and immune modulation and through systematic screening of clinically available options, three FDA-approved PARP inhibitors of Olaparib, Niraparib and Rucaparib were selected based on their established clinical profiles and therapeutic utility. It was systematically evaluated to identify the optimal candidate for chemotherapeutic combinations. Mechanistically, PARP inhibitors impede PARPase activity, thereby preventing the repair of DNA single-strand breaks, which subsequently accumulate and escalate into DNA double-strand breaks (DSBs).<sup>23</sup> As a hallmark of DSBs, phosphorylated histone H2AX ( $\gamma$ -H<sub>2</sub>AX) acts as a molecular sensor signaling their initiation and serves as a reliable indicator of DNA damage within cells.<sup>24</sup> Among the tested inhibitors, Olaparib treatment induced the most pronounced accumulation of DSBs in 4T1 cells, as evidenced by significantly elevated  $\gamma$ -H<sub>2</sub>AX expression (Fig. 1E). Quantitative analysis verified that  $\gamma$ -H<sub>2</sub>AX protein levels in the Olaparib-treated group were 1.73 times higher than those in the untreated control group (Fig. 1F). Based on these results, Olaparib demonstrated superior efficacy in disrupting DNA repair and enhancing DNA damage, thereby emerging as the most promising PARP-1 inhibitor for subsequent investigations aimed at integrating DNA repair disruption with immunomodulatory therapies. This selection paves the way for further studies on its potential to amplify antitumor immunity through cGAS-STING pathway activation.

### Synthesis and characterization of self-promoted tumor-targeting nanomedicine

Non-specific drug distribution significantly diminishes therapeutic efficacy and raises concerns regarding systemic toxicity. Additionally, the co-delivery of synergistic drug combinations to the same tumor cells enhances therapeutic outcomes by ensuring synchronized action. To address these challenges, a PD-L1-targeting peptide (WHRSYYTWNLNT) was employed,

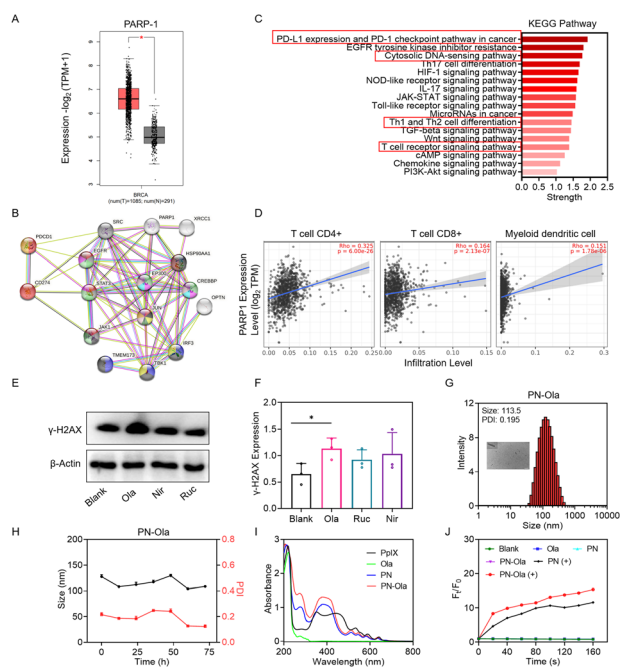


**Fig. 1** Bioinformatic analysis of PARP-1 in breast cancer and the fabrication of PN-Ola. (A) Differential expression of PARP-1 between breast cancer (BRCA) tissue and normal tissue was analyzed using the GEPIA database. (B) Protein-protein interaction (PPI) network associated with PARP-1. (C) Top 17 pathways identified through KEGG pathway enrichment analysis. (D) Correlation between PARP-1 expression and the infiltration of immune cells. (E) Western blot of  $\gamma$ -H<sub>2</sub>AX expression and (F) the quantitative analyses in 4T1 cells after treatment with Ola, Ruc and Nir. (G) Particle size and transmission electron microscopy (TEM) image of PN-Ola (scale bar: 1000 nm). (H) Changes in hydrodynamic size and polydispersity index (PDI) of PN-Ola over 72 hours ( $n = 3$ ). (I) UV-vis spectra of PpIX, Ola, PN, and PN-Ola. (J) Measurement of <sup>18</sup>O<sub>2</sub> production by Ola, PN, and PN-Ola, with or without light irradiation. \* $P < 0.05$  was tested *via* a Student's *t*-test.



which specifically binds PD-L1. This peptide serves a dual function: facilitating targeted drug delivery and acting as a PD-L1 blockade to counteract tumor immune evasion.<sup>25</sup> To enable amphiphilic modifications, hydrophobic palmitic acid and protoporphyrin IX (PpIX) were conjugated to the peptide *via* a lysine linker, forming a self-assembling photosensitizer-peptide conjugate (C<sub>16</sub>-K(PpIX)-WHRSSYTWNLNT, PN). PpIX functioned as a photosensitizer, generating reactive oxygen species (ROS) under light irradiation to damage DNA, activating the STING pathway and inducing immunogenic cell death (ICD) to enhance tumor immunogenicity. WHRSSYTWNLNT specifically bound PD-L1, enabling targeted delivery to PD-L1 overexpression tumor cells. PN was synthesized *via* solid-phase peptide synthesis, and its molecular weight was determined to be 1276.1 [M + 2H]<sup>2+</sup> using ESI-MS (Fig. S1, ESI†). Characterization confirmed that PN formed stable nano micelles with a particle size of 102.3 nm and a polydispersity index (PDI) of 0.198, maintaining stability for up to 72 hours (Fig. S2A and B, ESI†). Upon loading PN with the PARP inhibitor Ola, the resulting PN-Ola nanocomposite exhibited an increased particle size of 113.5 nm and a PDI of 0.195. TEM imaging confirmed its rod-shaped nanostructure, and PN-Ola demonstrated remarkable stability in water over 72 hours, with a PDI below 0.3 (Fig. 1G and H). UV-vis absorption spectra verified characteristic peaks of PpIX at 400 nm and 530 nm, confirming successful drug loading (Fig. 1I). Following that, the zeta potential of PN-Ola was evaluated to be about 21.40 mV (Fig. S3, ESI†). Quantitative analysis by HPLC and UV-vis spectrophotometry determined the concentrations of PN and Ola in PN-Ola to be 1278.0 mg L<sup>-1</sup> and 52.7 mg L<sup>-1</sup>, respectively (Fig. S4A and B, ESI†). Furthermore, the stability and drug release profile of PN-Ola under physiological conditions were evaluated. PN-Ola maintained its size and PDI in 10% serum and PBS for over 60 hours, demonstrating excellent *in vivo* stability and biocompatibility (Fig. S5A and B, ESI†). Moreover, over 90% of Ola was released from PN-Ola in PBS, confirming its efficient drug release capabilities (Fig. S5C, ESI†). The production of singlet oxygen (<sup>1</sup>O<sub>2</sub>) by PN-Ola was assessed using a SOSG fluorescent probe. Following light exposure, the PN-Ola group exhibited a remarkable <sup>1</sup>O<sub>2</sub> generation capacity, 15-fold greater than the control group (Fig. 1J). These results highlighted the superior photodynamic and drug delivery properties of PN-Ola, establishing a robust foundation for its application in breast cancer therapy.

### Self-promoted tumor targeting behavior of PN-Ola *in vitro*

The internalization behavior of PN-Ola was assessed in breast cancer cells, with normal cells serving as controls. Cellular uptake was examined in three cell lines: 3T3, L929, and 4T1. Confocal microscopy revealed that PN-Ola (red fluorescence) was internalized by all three cell types after 8 hours of incubation, with the highest intensity observed in 4T1 cells (Fig. 2A). This finding indicated a preferential uptake of PN-Ola by 4T1 cells, a trend confirmed by fluorescence quantification over different incubation times (2, 4, and 8 hours). Specifically, at 8 hours, the uptake of PN-Ola in 4T1 cells was significantly greater

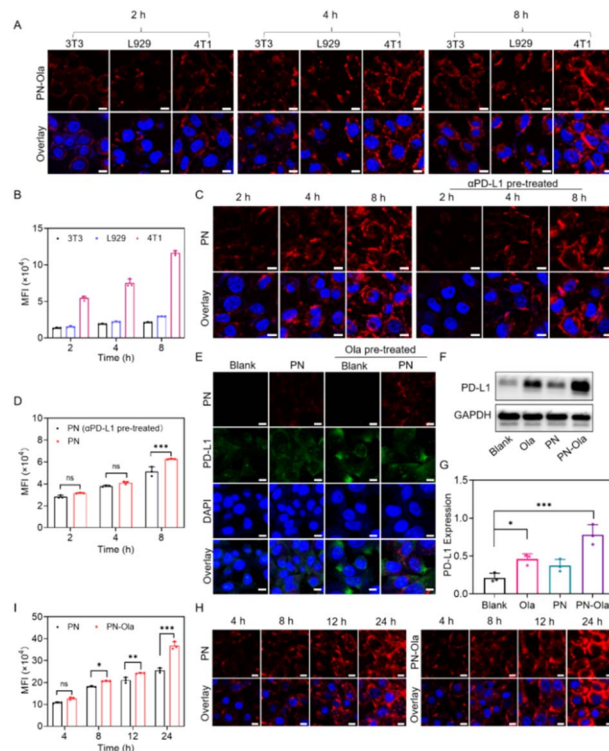


Fig. 2 Self-promoted tumor targeting behavior of PN-Ola *in vitro*. (A) CLSM images showed the cellular uptake of PN-Ola in 3T3, L929, and 4T1 cells at various time points. Scale bar: 10  $\mu$ m. (B) Flow cytometry analysis of cellular uptake in 3T3, COS7, and 4T1 cells. (C) Time-dependent CLSM images of PN uptake in 4T1 cells, with pre-treatment of anti-PD-L1 antibody for 24 hours as a control. Scale bar: 10  $\mu$ m. (D) Flow cytometry analysis of PN uptake in 4T1 cells and anti-PD-L1 antibody pre-treated 4T1 cells. (E) CLSM images of PN uptake in 4T1 cells with or without Ola pretreatment, along with PD-L1 expression visualization. Scale bar: 10  $\mu$ m. (F) Western blot analysis of PD-L1 expression. (G) Quantitative analysis of PD-L1 expression after treatment with Ola, PN, and PN-Ola. (H) CLSM images of 4T1 cellular uptake after treatment with PN or PN-Ola at different time points. Scale bar: 10  $\mu$ m. (I) Flow cytometry analysis of 4T1 cellular uptake after treatment with PN or PN-Ola at various time points. \* $P$  < 0.05, \*\* $P$  < 0.01 and \*\*\* $P$  < 0.001 were determined using a Student's  $t$ -test.

than in 3T3 and L929 cells, with 4T1 uptake being 4.4-fold and 3.9-fold higher than in 3T3 and L929, respectively (Fig. 2B). The enhanced uptake in 4T1 cells was hypothesized to result from the high expression of PD-L1, enabling PN-Ola to selectively target and bind PD-L1. When employing PN-Ola nanomedicine, this Ola-mediated PD-L1 regulation could potentially influence cellular internalization characteristics. Therefore, PN was utilized to confirm the PD-L1 specificity of PN-Ola, cells were pretreated with an anti-PD-L1 antibody to block PD-L1 on the cell surface. This pretreatment markedly reduced PN uptake, supporting that PN enters cells *via* PD-L1 receptor-mediated endocytosis (Fig. 2C). Quantitative analysis showed that untreated 4T1 cells internalized 22% more PN compared to cells pretreated with the anti-PD-L1 antibody after 8 hours of incubation (Fig. 2D). These results demonstrated the efficacy of surface engineering with a PD-L1-targeting peptide sequence in promoting the selective targeting and internalization of PN-Ola



into breast cancer cells. This targeted delivery strategy not only enhanced drug accumulation in cancer cells but also minimized off-target effects, highlighting its potential for precise breast cancer therapy.

Developing self-promoting tumor-targeting strategies to enhance drug delivery effectiveness could complement the use of tailored nanodrugs for targeted tumor therapy. PARP inhibitors, such as Ola, are known to induce DNA damage and activate the STING-TBK1-IRF3 pathway in tumors, which subsequently upregulates PD-L1 expression.<sup>26,27</sup> As shown in Fig. 2E, baseline PD-L1 expression was observed in untreated cells, while pretreatment with Ola significantly elevated PD-L1 levels in both the blank and PN-treated cells. Immunoblotting results further confirmed that Ola-treated cells exhibited an elevated PD-L1 protein level, with PN-Ola-treated cells displaying the highest expression (Fig. 2F). Quantitative analysis showed a 2.14-fold increase in PD-L1 protein in the Ola group compared to the blank group, and a remarkable 3.66-fold increase in the PN-Ola group (Fig. 2G). These findings indicated that PN-Ola not only facilitates active targeting of PD-L1 but also enhances PD-L1 expression *via* Ola-induced pathways, promoting a positive feedback loop that sustains nanomedicine uptake by tumor cells. To validate this self-promoted mechanism, cellular uptake of PN and PN-Ola was compared at various time points. PN-Ola uptake was consistently and significantly higher than that of PN alone, with increases of 17.5%, 14.0%, 15.0%, and 43.5% observed over PN at different incubation times (Fig. 2H and I). These findings collectively demonstrated that PN-Ola effectively targets PD-L1, promoting its endocytosis by tumor cells. Additionally, the Ola component induces upregulation of PD-L1 expression, establishing a positive feedback loop that enhances the active targeting capability of PN-Ola. This self-promoting mechanism significantly improved the internalization and bioavailability of PN-Ola within tumors, providing a promising strategy to enhance drug delivery efficiency while addressing the heterogeneous distribution and personalized variations of PD-L1.

### Anti-proliferation ability of PN-Ola

The oxidative damage to proteins, lipids, and DNA significantly contributes to the antiproliferative effects of PDT, where the cytotoxicity of a photosensitizer is primarily determined by its ROS production capacity.<sup>28</sup> To evaluate the ROS generation ability of PN-Ola, cells were treated with the DCFH-DA fluorescent probe. As shown in Fig. 3A, distinct green fluorescence was observed in the PN (+) and PN-Ola (+) groups, indicating robust ROS production. Quantitative analysis further confirmed that significant ROS generation occurred only in the light-exposed PN and PN-Ola groups, whereas negligible ROS was detected in the other groups (Fig. S6, ESI†). Subsequently, the anti-proliferation ability of PN-Ola was assessed by using a live/dead cell staining assay. As illustrated in Fig. 3B, live cells are marked by green fluorescence and dead cells by red fluorescence, with an evident increase in cell death following laser irradiation. Red fluorescence was considerably greater in the PN (+) and PN-Ola (+) groups relative to the non-laser treatment

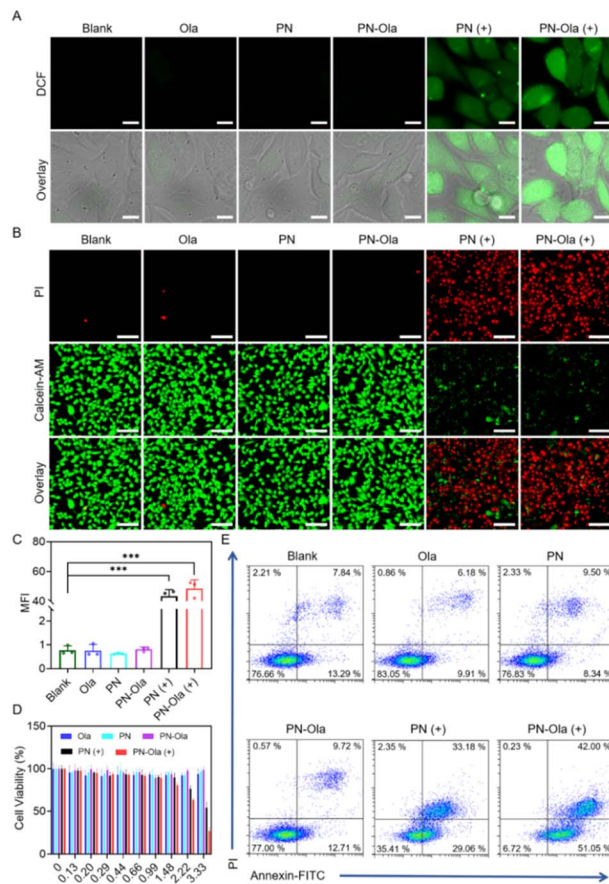


Fig. 3 Anti-proliferation ability of PN-Ola. (A) CLSM images of 4T1 cells treated with Ola, PN, and PN-Ola with or without light irradiation, using DCFH-DA as the indicator. Scale bar: 10  $\mu\text{m}$ . (B) CLSM images and (C) mean fluorescence intensity (MFI) analysis of 4T1 cells after live/dead cell staining following treatment with Ola, PN, and PN-Ola in the presence or absence of light irradiation. Scale bar: 100  $\mu\text{m}$ . (D) Viability of 4T1 cells after treatment with Ola, PN, and PN-Ola, with or without light irradiation. (E) Apoptosis analysis of 4T1 cells by flow cytometry after treatment with Ola, PN, and PN-Ola under dark or light irradiation (8 min). Light irradiation is denoted by "+". \*\*\* $P < 0.001$  was determined by a Student's *t*-test.

group. Quantitative analysis showed a pronounced tumor-killing effect in the PN-Ola (+) group, surpassing that of the PN (+) group (Fig. 3C). This enhanced cytotoxicity was likely attributed to the synergistic effects of PN and Ola in inducing DNA damage in tumor cells. Remarkably, the survival rate of cells treated with PN-Ola (+) was reduced to just 27% at a concentration of 3.33  $\text{mg L}^{-1}$  (Fig. 3D). PN-Ola dark treatment had no PDT effect, which might not be reflected by cytotoxicity at low doses *in vitro*. To further elucidate the cell death mechanism, the Annexin V-FITC/PI assay was performed to evaluate apoptosis rates across different treatment groups. Following laser irradiation, both early and late apoptosis rates were significantly increased in treated cells compared with the blank group (Fig. 3E). Specifically, the PN-Ola (+) group exhibited a late apoptosis rate of 42.00%, an early apoptosis rate of 51.05%, and a cell survival rate of only 6.72%. These results collectively demonstrated that PN-Ola, upon laser activation,



induced potent tumor cell-killing effects by enhancing ROS generation and synergizing with Ola-induced DNA damage, significantly outperforming the other treatments.

### Activation of the STING pathway *in vitro*

PARP in tumor cells plays a critical role in repairing ROS-induced DNA damage, potentially limiting the therapeutic efficacy of PDT.<sup>29,30</sup> As a PARP inhibitor, Ola suppresses the repair of single-strand DNA breaks, leading to the formation of more severe DSBs. To evaluate DSB formation, immunofluorescence staining for  $\gamma$ -H<sub>2</sub>AX, a marker of DNA damage, was performed. As shown in Fig. 4A, moderate  $\gamma$ -H<sub>2</sub>AX production was observed in the Ola-containing and PN (+) groups, while the PN-Ola (+) group exhibited the highest  $\gamma$ -H<sub>2</sub>AX levels. Quantitative fluorescence analysis further confirmed a notable 18.8% increase in  $\gamma$ -H<sub>2</sub>AX generation in the PN-Ola (+) group compared to the PN (+) group, indicating a significantly elevated occurrence of DSBs (Fig. S7, ESI†). Additionally, the blank and PN groups produced minimal  $\gamma$ -H<sub>2</sub>AX, demonstrating that DSB formation primarily results from the combined effects of PDT and Ola (Fig. 4B). Protein expression analysis corroborated these findings, with PN-Ola (+) showing a 4.6-fold increase in  $\gamma$ -H<sub>2</sub>AX levels compared to the blank group (Fig. 4C). These results suggested that the integration of PDT and Ola in the PN-Ola exerts a remarkable synergistic effect, promoting apoptosis and inducing substantial DSBs in tumor cells.

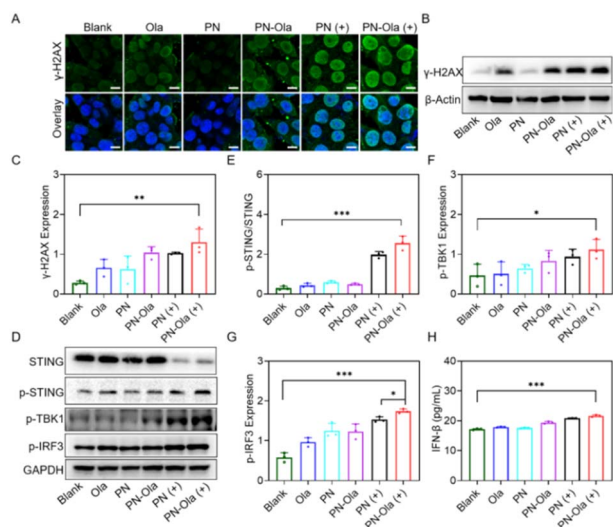


Fig. 4 Activation of the STING pathway *in vitro*. (A) Immunofluorescence staining of  $\gamma$ -H<sub>2</sub>AX in 4T1 cells after various treatments with or without light irradiation. Scale bar: 10  $\mu$ m. (B) Western blot analysis of  $\gamma$ -H<sub>2</sub>AX expression, (C) and corresponding quantitative analysis following treatment with Ola, PN, and PN-Ola, in the presence or absence of light irradiation. (D) Expression of STING, p-STING, p-TBK1, and p-IRF3 in DC cells co-cultured with 4T1 tumor cells treated with different agents, as determined by Western blot. (E) Quantitative analysis of p-STING/STING, (F) p-TBK1, and (G) p-IRF3 expressions. (H) IFN- $\beta$  expression in DC cells collected from the DC/4T1 co-culture medium, measured by ELISA. Light irradiation is denoted by "+". \* $P$  < 0.05, \*\* $P$  < 0.01 and \*\*\* $P$  < 0.001 were determined using a Student's  $t$ -test.

Beyond inducing DNA damage, antigen-presenting cells (APCs), such as DCs, play an essential role in orchestrating the immune response. DCs recognize tumor-derived double-stranded DNA (dsDNA) fragments or cyclic GMP-AMP (cGAMP), thereby initiating the STING-driven type I interferon (IFN) signaling pathway. This pathway involves the recruitment of tank-binding kinase 1 (TBK1) by STING, leading to TBK1-mediated phosphorylation and activation of interferon regulatory factor 3 (IRF3), which subsequently drives the expression of IFNs and chemokines. To assess the activation of DCs and the STING pathway, co-cultures of DCs with 4T1 tumor cells pre-treated with various formulations were analyzed for key protein expressions in the STING signaling cascade. Western blot results indicated that the PN-Ola (+) group displayed a slight decrease in total STING levels but a substantial increase in phosphorylated STING (p-STING) levels (Fig. 4D). Furthermore, the expression of downstream phosphorylated proteins (p-TBK1 and p-IRF3) was markedly upregulated. Quantitative analysis demonstrated that the PN-Ola (+) group exhibited the highest p-STING/STING ratio, with a 2.4-fold increase in p-TBK1 levels relative to the blank group and a 13.9% elevation in p-IRF3 levels compared to the PN (+) group (Fig. 4E-G). To further evaluate the functional impact of STING activation, the production of interferon-beta (IFN- $\beta$ ) was measured in the supernatants of co-cultured tumor cells and DCs. The PN-Ola (+) group displayed a 26.0% increase in IFN- $\beta$  secretion compared to the blank group (Fig. 4H). These findings robustly established that PN-Ola (+) effectively activated the STING signaling pathway, verifying its potential to enhance DC-mediated immune responses and drive the expression of pro-inflammatory cytokines.

### Anti-tumor capability of PN-Ola *in vivo*

Before assessing the anti-tumor potential, the biodistribution and tumor-targeting behavior of PN-Ola were evaluated using a fluorescence imaging system. As illustrated in Fig. 5A, fluorescence signals at the tumor site progressively increased over time, peaking at 24 hours post-administration. Similarly, fluorescence signals were observed in excised tumors after 24 hours. This result suggests that PN-Ola effectively enhances drug accumulation at tumor sites, which could be attributed to the PD-L1-targeting peptides and the self-promoted tumor-targeting capability of PN-Ola. Subsequently, the anti-tumor efficacy of PN-Ola was investigated in 4T1 tumor-bearing mice. On the 7th day post-tumor inoculation, the mice were randomly assigned to different treatment groups. Tumor volumes and body weights were monitored throughout the treatment course, with therapeutic outcomes evaluated on the 30th day. The PN-Ola (+) group exhibited significantly suppressed tumor growth, with a 57.2% reduction in tumor volume compared to the PN (+) group (Fig. 5B). Representative tumor images from each group confirmed this trend, with complete tumor regression observed in individual PN-Ola (+) mice (Fig. 5C). Consistent with these observations, tumor weights in the PN-Ola (+) group were halved relative to the PN (+) group (Fig. 5D). These findings highlighted the superior tumor-



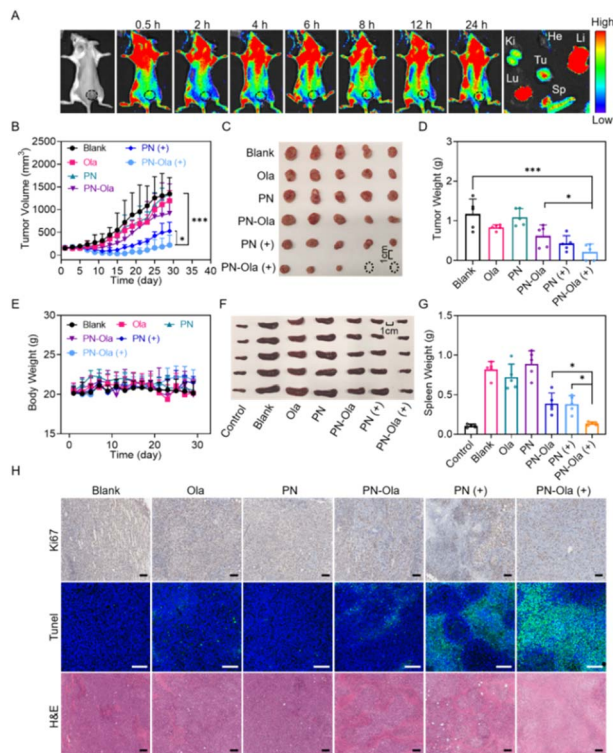


**Fig. 5** Anti-tumor capability of PN-Ola *in vivo*. (A) Real-time fluorescence imaging of mice after intravenous injection of PN-Ola at 0.5, 2, 4, 6, 8, 12, and 24 hours, along with tissue imaging at 24 hours post-injection. (B) Relative tumor volume changes in mice after treatment with Ola, PN, and PN-Ola, with or without light irradiation. (C) Tumor tissue images from sacrificed mice, and (D) corresponding tumor weights after various treatments. (E) Changes in the body weight of mice following different treatments. (F) Spleen images from sacrificed mice, and (G) corresponding spleen weights after treatment with Ola, PN, and PN-Ola in the presence or absence of light irradiation. (H) Ki67, TUNEL, and H&E staining of tumor tissues following various treatments. Scale bar: 100  $\mu\text{m}$ . Light irradiation is denoted by "+". \* $P < 0.05$  and \*\*\* $P < 0.001$  were determined using a Student's *t*-test.

targeting and therapeutic efficacy of PN-Ola, demonstrating its potential as an effective strategy for cancer treatment by leveraging the dual benefits of targeted delivery and synergistic therapeutic mechanisms.

Throughout the treatment period, no significant changes in body weight were observed in any of the groups, indicating that PN-Ola exhibits good biocompatibility and negligible systemic toxicity *in vivo* (Fig. 5E). Tumor progression is often associated with splenomegaly due to its impact on immune regulation and systemic inflammation.<sup>31</sup> Therefore, spleens from mice treated with different formulations were assessed. Notably, the PN-Ola (+) group displayed spleen sizes comparable to those of healthy mice, whereas the other treatment groups showed varying degrees of splenomegaly (Fig. 5F). Additionally, the spleen weight in the PN-Ola (+) group was significantly reduced, showing a 64.5% decrease compared to the PN (+) group and closely aligning with that of healthy controls (Fig. 5G). Histological analyses further corroborated the robust therapeutic efficacy of PN-Ola (+). Ki67 staining also verified the lowest

proliferation index in the PN-Ola (+) group, signifying minimal tumor cell proliferation and a markedly slower tumor growth rate compared to the other groups. Moreover, TUNEL staining demonstrated the highest levels of tumor cell apoptosis in the PN-Ola (+) group (Fig. 5H). Collectively, these findings underscored the potent tumor-suppressive effects of PN-Ola (+), further emphasizing the synergistic therapeutic advantages of integrating PDT with PARP inhibition.

### Immune activation of PN-Ola for metastatic tumor eradication

Breast cancer, a malignancy with a strong propensity for lung metastasis, is further marked by its high motility and invasiveness.<sup>32</sup> Given the STING activation ability of PN-Ola, its effect on inhibiting metastatic tumors and the underlying mechanisms were explored. As shown in Fig. 6A, images of lung tissue and H&E staining revealed that 4T1 tumors rapidly metastasized to the lungs in the blank and other treatment groups, forming numerous visible metastatic nodules. In contrast, metastatic nodules were nearly absent in the PN-Ola

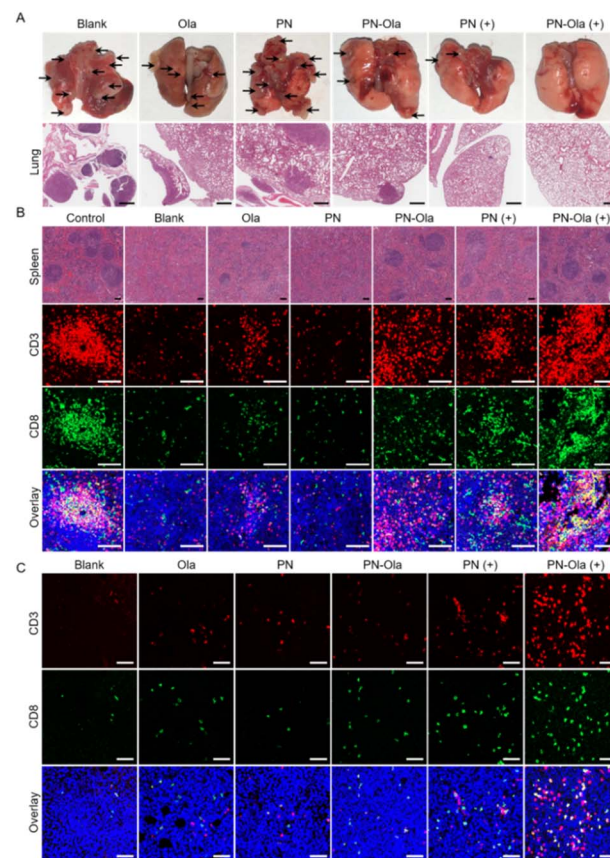


**Fig. 6** Immune activation of PN-Ola for metastatic tumor eradication *in vivo*. (A) Images of lung metastatic nodes and H&E staining of lung tissues in mice after treatment with Ola, PN, and PN-Ola. Scale bar: 600  $\mu\text{m}$ . (B) H&E staining of spleen tissues and CD3<sup>+</sup>CD8<sup>+</sup> cell infiltration after treatment with Ola, PN, and PN-Ola with or without light irradiation. Scale bar: 50  $\mu\text{m}$ . (C) CD3<sup>+</sup>CD8<sup>+</sup> cell infiltration in tumors after treatment with Ola, PN, and PN-Ola with or without light irradiation. Scale bar: 50  $\mu\text{m}$ . Light irradiation is denoted by "+".



(+) group. Corresponding H&E staining results demonstrated a dramatic reduction in lung metastases, emphasizing the potent anti-metastatic efficacy of PN-Ola (+). Further analysis indicated that PN-Ola (+) treatment induced the highest levels of CD8<sup>+</sup> T cells in lung tissue (Fig. S8, ESI†). As we know, the spleen is primarily composed of red and white pulp, with the latter serving as a hub for specific immune responses.<sup>33</sup> H&E staining confirmed a clear boundary between the red and white pulp in the PN-Ola (+) group, coupled with a substantial increase in white pulp comparable to healthy mice (Fig. 6B). In contrast, the other groups exhibited a blurred boundary and diminished white pulp, indicating impaired immune function. This effect correlated with an increase in CD8<sup>+</sup> T cells, as evidenced by the strong co-localization of red and green fluorescence in spleen tissue from the PN-Ola (+) group, surpassing levels observed in the other treatments and even approaching those in healthy mice. These findings collectively evidenced the ability of PN-Ola (+) to inhibit lung metastasis while boosting systemic immune responses, particularly through the recruitment and activation of CD8<sup>+</sup> T cells.

Additionally, tumor tissues treated with PN-Ola (+) exhibited significantly increased CD8<sup>+</sup> T cell infiltration compared to all other groups, confirming its potent immune activation capacity (Fig. 6C). To further explore the underlying mechanism, PD-L1 expression levels were quantified. In groups treated with Ola-containing formulations, a consistent upregulation of PD-L1 was observed. Notably, PN-Ola and PN-Ola (+) exhibited the highest PD-L1 expression, likely due to the active targeting capabilities of PN-Ola, which facilitated enhanced drug accumulation and immune modulation at the tumor site (Fig. S9, ESI†). This upregulation of PD-L1 created a favorable microenvironment for the self-promoted tumor-targeting activity of PN-Ola, further supporting enhanced T-cell infiltration within the tumor beds. Collectively, these findings highlighted that PN-Ola (+) not only activated systemic anti-tumor immunity to eliminate metastatic tumors but also accelerated T-cell infiltration, demonstrating significant potential to enhance the overall immunotherapeutic response.

### Immunotherapeutic response of PN-Ola

A 4T1 mouse hormonal tumor model was established to evaluate the immunotherapeutic response of PN-Ola, and the treatment schedule is outlined in Fig. 7A. Cytotoxic CD8<sup>+</sup> T cells, which play a crucial role in tumor elimination, require CD4<sup>+</sup> T cells for immune response maintenance and to prevent depletion during anti-tumor therapies.<sup>34</sup> To better understand the *in vivo* immune response, the differentiation of T-cell subpopulations in the spleens and tumors of mice was assessed to reflect the activation of the systemic immune system. Flow cytometry results demonstrated a notable expansion of CD4<sup>+</sup> T cells in the spleen in the PN-Ola, PN (+), and PN-Ola (+) groups, with the PN-Ola (+) group showing the highest increase, exhibiting a 22.3% enhancement over the PN (+) group (Fig. 7B). Similarly, the PN-Ola (+) group had a significantly larger number of CD8<sup>+</sup> T cells compared to the other groups, with increases of 2.9 and 1.8 times over the blank and PN (+) groups, respectively (Fig. 7C). In

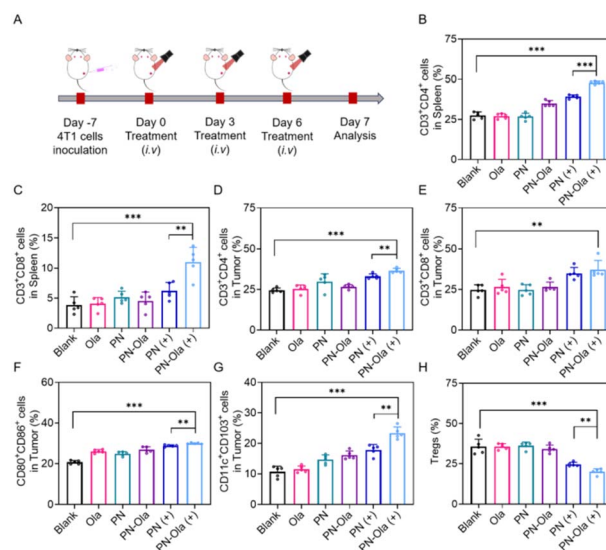
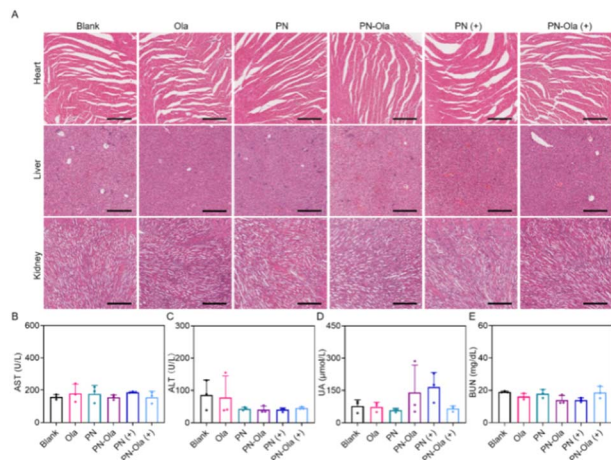


Fig. 7 Immunotherapeutic response of PN-Ola. (A) Therapeutic schedule of PN-Ola in 4T1 tumor-bearing mice. (B) CD3<sup>+</sup>CD4<sup>+</sup> T cell population and (C) CD3<sup>+</sup>CD8<sup>+</sup> T cell population in the spleen after treatment with Ola, PN, and PN-Ola with or without light irradiation. (D) CD3<sup>+</sup>CD4<sup>+</sup> T cell population and (E) CD3<sup>+</sup>CD8<sup>+</sup> T cell population in tumors after treatment with Ola, PN, and PN-Ola with or without light irradiation. (F) CD80<sup>+</sup>CD86<sup>+</sup> cells and (G) CD11c<sup>+</sup>CD103<sup>+</sup> dendritic cells in tumors after treatment with Ola, PN, and PN-Ola with or without light irradiation. (H) Treg cell population in tumors after treatment with Ola, PN, and PN-Ola with or without light irradiation. Light irradiation is denoted by "+". \**P* < 0.05, \*\**P* < 0.01 and \*\*\**P* < 0.001 were tested using a Student's *t*-test.

addition to systemic immune activation, lymphocyte infiltration within the tumor microenvironment was further evaluated. The PN-Ola (+) group exhibited the highest infiltration of both CD4<sup>+</sup> and CD8<sup>+</sup> T cells into the tumor site. The proportion of these T cells increased by 10.8% and 6.6% compared to the PN (+) group (Fig. 7D and E). These results confirmed the robust immune activation ability of PN-Ola (+). These findings highlighted the robust immune activation capability of PN-Ola (+), supporting its potential as an effective immunotherapeutic approach.

Mature DCs, after antigen capture and activation, reside in lymph nodes to stimulate and activate T cells, playing a pivotal role in anti-tumor immunity.<sup>35</sup> In the tumor microenvironment, PN-Ola (+) significantly enhanced the expression of co-stimulatory markers CD80<sup>+</sup> and CD86<sup>+</sup> on DCs, indicating improved antigen presentation and co-stimulation ability (Fig. 7F). Furthermore, CD103<sup>+</sup> DCs, a subset of APCs critical for T cell trafficking and immunity initiation, increased by 1.31 times at the tumor site following PN-Ola (+) treatment compared to the PN (+) group (Fig. 7G). Regulatory T cells (Tregs), which are known to suppress immune responses, were significantly reduced in both the PN (+) and PN-Ola (+) groups. Notably, the proportion of Tregs in the PN-Ola (+) group was 23.1% lower than that in the PN (+) group, suggesting that the tumor immune suppression was alleviated (Fig. 7H). Collectively, these findings demonstrated that PN-Ola treatment induces a potent anti-tumor immune response by stimulating dendritic cells and lymphocyte activation, enhancing T-cell





**Fig. 8** Biosafety analysis of PN-Ola. (A) H&E staining of heart, liver, and kidney tissues after treatment with Ola, PN, and PN-Ola with or without light irradiation. Scale bar: 300 μm. Biochemical analysis of (B) AST, (C) ALT, (D) UA, and (E) BUN levels in mice after treatment with Ola, PN, and PN-Ola with or without light irradiation. Light irradiation is denoted by "+".

infiltration, and reducing Treg-mediated suppression. This robust intratumoral and systemic immune activation supported the therapeutic potential of PN-Ola in promoting immunotherapeutic response.

### Biosafety analysis of PN-Ola

To evaluate the systemic toxicity of the treatment, the major organs from all groups of mice were harvested after the treatment. Histopathological analysis using H&E staining found no significant changes in the organ structure of any treatment group, indicating the absence of notable organ damage following PN-Ola treatment (Fig. 8A). In addition to histopathological assessment, serum levels of aspartate aminotransferase (AST), alanine aminotransferase (ALT), uric acid (UA), and blood urea nitrogen (BUN) were measured. Hematological analyses showed that the levels of these parameters were within the normal range for all treated groups, with no abnormal indicators detected (Fig. 8B–E). These findings suggested that PN-Ola exhibited excellent biocompatibility and biosafety *in vivo*, with minimal side effects and toxicity. Overall, these results support the favorable safety profile of PN-Ola, further highlighting its significant advantage in activating anti-tumor immunity while avoiding side effects.

## Conclusions

In this study, bioinformatic analysis confirmed the abnormal expression of PARP-1 in breast cancer, closely associated with the cGAS-STING signaling pathway and immunosuppressive behavior. Additionally, Ola was identified as the most effective PARP-1 inhibitor to amplify DNA damage, thereby enhancing the immunotherapeutic response in breast cancer. Based on these mechanistic insights, a self-promoted tumor-targeting nanomedicine of PN-Ola was fabricated to activate STING-

driven antitumor immunity through photodynamic DNA damage and PARP inhibition. PN-Ola selectively accumulates in tumor cells overexpressing PD-L1, while also upregulating PD-L1 expression, thereby creating a feedback loop that self-promotes drug delivery efficiency. The PDT effects of PN-Ola generate substantial ROS within tumor cells, inducing oxidative DNA damage and the subsequent accumulation of DNA fragments to activate STING-mediated antitumor immunity. The synergistic mechanism of PN-Ola effectively boosts the immunotherapeutic response by enhancing T cell activation and infiltration, resulting in the eradication of metastatic tumors without inducing side effects. This study presents a promising strategy to overcome targeting ligand heterogeneity, while simultaneously activating systemic antitumor immunity for the effective elimination of metastatic tumors.

## Ethical statement

All experiments were performed in accordance with the guidelines for the care and use of laboratory animals provided by the Animal Research Committee of Guangzhou Medical University and approved by the Ethics Committee of Guangzhou Medical University (Approval No. GY2024-286). Informed consents were obtained from human participants of this study. Animal models were constructed by subcutaneous injection of 4T1 cells into the right hind leg of female BALB/c mice.

## Data availability

Essential data are fully provided in the main text and ESI.†

## Author contributions

Baixue Yu: conceptualization, investigation, data curation, writing – original draft. Wei Zhang: methodology, investigation. Zhouchuan Shao: investigation. Xiayun Chen: investigation. Yi Cen: investigation. Yibin Liu: investigation. Ying Chen: investigation. Xinxuan Li: investigation. Ziqi Liang: investigation. Shiyong Li: conceptualization, funding acquisition, writing – review & editing. Xiaoyuan Chen: conceptualization, project administration, supervision.

## Conflicts of interest

There are no conflicts to declare.

## Acknowledgements

This work was financially supported by the National Natural Science Foundation of China (32371394), the National Key R&D Program of China (2021YFD1800600), the Special Projects in Key Areas of Colleges and Universities in Guangdong Province (2022ZDZX2046), the Guangdong Basic and Applied Basic Research Foundation (2023A1515140078), and the Open Project of State Key Laboratory of Respiratory Disease (SKLRD-OP-202502). S. Y. Li acknowledges the financial support from the China Scholarship Council for foreign research and life.



## Notes and references

- 1 Q. Chen, L. Sun and Z. J. Chen, *Nat. Immunol.*, 2016, **17**, 1142–1149.
- 2 X. Zhang, X. C. Bai and Z. J. Chen, *Immunity*, 2020, **53**, 43–53.
- 3 L. L. Cao and J. C. Kagan, *Immunity*, 2023, **56**, 2206–2217.
- 4 Z. S. Guo, B. Lu, Z. Guo, E. Giehl, M. Feist, E. Dai, W. Liu, W. J. Storkus, Y. He, Z. Liu and D. L. Bartlett, *J. Immunother. Cancer*, 2019, **7**, 6.
- 5 L. Yang, A. Li, Y. Wang and Y. Zhang, *Signal Transduction Targeted Ther.*, 2023, **8**, 35.
- 6 M. Overchuk, R. A. Weersink, B. C. Wilson and G. Zheng, *ACS Nano*, 2023, **17**, 7979–8003.
- 7 W. Wang, C. Zhu, B. Zhang, Y. Feng, Y. Zhang and J. Li, *J. Am. Chem. Soc.*, 2023, **145**, 16642–16649.
- 8 X. Hu, M. Zhang, C. Quan, S. Ren, W. Chen and J. Wang, *Bioact. Mater.*, 2024, **36**, 490–507.
- 9 A. Zhang, A. Gao, C. Zhou, C. Xue, Q. Zhang, J. M. Fuente and D. Cui, *Adv. Mater.*, 2023, **35**, e2303722.
- 10 J. Yang, B. Ren, X. Yin, L. Xiang, Y. Hua, X. Huang, H. Wang, Z. Mao, W. Chen and J. Deng, *Adv. Mater.*, 2024, **36**, e2402720.
- 11 T. Wang, J. Tao, B. Wang, T. Jiang, X. Zhao, Y. Yu and X. Meng, *Adv. Healthcare Mater.*, 2024, **13**, e2302597.
- 12 C. Pantelidou, O. Sonzogno, M. De Oliveria Taveira, A. K. Mehta, A. Kothari, D. Wang, T. Visal, M. K. Li, J. Pinto, J. A. Castrillon, E. M. Cheney, P. Bouwman, J. Jonkers, S. Rottenberg, J. L. Guerriero, G. M. Wulf and G. I. Shapiro, *Cancer Discovery*, 2019, **9**, 722–737.
- 13 T. Sen, B. L. Rodriguez, L. Chen, C. M. D. Corte, N. Morikawa, J. Fujimoto, S. Cristea, T. Nguyen, L. Diao, L. Li, Y. Fan, Y. Yang, J. Wang, B. S. Glisson, I. I. Wistuba, J. Sage, J. V. Heymach, D. L. Gibbons and L. A. Byers, *Cancer Discovery*, 2019, **9**, 646–661.
- 14 Q. Wang, J. S. Bergholz, L. Ding, Z. Lin, S. K. Kabraji, M. E. Hughes, X. He, S. Xie, T. Jiang, W. Wang, J. J. Zoeller, H. J. Kim, T. M. Roberts, P. A. Konstantinopoulos, U. A. Matulonis, D. A. Dillon, E. P. Winer, N. U. Lin and J. J. Zhao, *Nat. Commun.*, 2022, **13**, 3022.
- 15 Z. Zhao, A. Ukidve, J. Kim and S. Mitragotri, *Cell*, 2020, **181**, 151–167.
- 16 X. Yu, Y. Long, B. Chen, Y. Tong, M. Shan, X. Jia, C. Hu, M. Liu, J. Zhou, F. Tang, H. Lu, R. Chen, P. Xu, W. Huang, J. Ren, Y. Wan, J. Sun, J. Li, G. Jin and L. Gong, *J. Immunother. Cancer*, 2022, **10**, e004590.
- 17 M. Bajor, A. Graczyk-Jarzynka, K. Marhelava, A. Burdzinska, A. Muchowicz, A. Goral, A. Zhytko, K. Soroczynska, K. Retecki, M. Krawczyk, M. Klopowska, Z. Pilch, L. Paczek, K. J. Malmberg, S. Wälchli, M. Winiarska and R. Zagodzón, *J. Immunother. Cancer*, 2022, **10**, e002500.
- 18 X. Wang, X. Yang, C. Zhang, Y. Wang, T. Cheng, L. Duan, Z. Tong, S. Tan, H. Zhang, P. E. Saw, Y. Gu, J. Wang, Y. Zhang, L. Shang, Y. Liu, S. Jiang, B. Yan, R. Li, Y. Yang, J. Yu, Y. Chen, G. F. Gao, Q. Ye and S. Gao, *Proc. Natl. Acad. Sci. U. S. A.*, 2020, **117**, 6640–6650.
- 19 H. K. Gan, A. W. Burgess, A. H. Clayton and A. M. Scott, *Cancer Res.*, 2012, **72**, 2924–2930.
- 20 Y. Zhu, S. H. Choi and K. Shah, *Lancet Oncol.*, 2015, **16**, e543–e554.
- 21 J. D. Domizio, M. F. Gulen, F. Saidoune, V. V. Thacker, A. Yatim, K. Sharma, T. Nass, E. Guenova, M. Schaller, C. Conrad, C. Goepfert, L. de Leval, C. V. Garnier, S. Berezowska, A. Dubois, M. Gilliet and A. Ablasser, *Nature*, 2022, **603**, 145–151.
- 22 H. Brown Harding, G. N. Kwaku, C. M. Reardon, N. S. Khan, D. Zamith-Miranda, R. Zarnowski, J. M. Tam, C. K. Bohaen, L. Richey, K. Mosallanejad, A. J. Crossen, J. L. Reedy, R. A. Ward, D. A. Vargas-Blanco, K. J. Basham, R. P. Bhattacharyya, J. E. Nett, M. K. Mansour, F. L. van de Veerdonk, V. Kumar, J. C. Kagan, D. R. Andes, J. D. Nosanchuk and J. M. Vyas, *Nat. Microbiol.*, 2024, **9**, 95–107.
- 23 M. Petropoulos, A. Karamichali, G. G. Rossetti, A. Freudenmann, L. G. Iacovino, V. S. Dionellis, S. K. Sotiriou and T. D. Halazonetis, *Nature*, 2024, **628**, 433–441.
- 24 J. Yuan, R. Adamski and J. Chen, *FEBS Lett.*, 2010, **584**, 3717–3724.
- 25 H. Liu, Z. Zhao, L. Zhang, Y. Li, A. Jain, A. Barve, W. Jin, Y. Liu, J. Fetse and K. Cheng, *J. Immunother. Cancer*, 2019, **7**, 270.
- 26 T. Sen, B. L. Rodriguez, L. Chen, C. M. D. Corte, N. Morikawa, J. Fujimoto, S. Cristea, T. Nguyen, L. Diao, L. Li, Y. Fan, Y. Yang, J. Wang, B. S. Glisson, I. I. Wistuba, J. Sage, J. V. Heymach, D. L. Gibbons and L. A. Byers, *Cancer Discovery*, 2019, **9**, 646–661.
- 27 S. Jiao, W. Xia, H. Yamaguchi, Y. Wei, M. K. Chen, J. M. Hsu, J. L. Hsu, W. H. Yu, Y. Du, H. H. Lee, C. W. Li, C. K. Chou, S. O. Lim, S. S. Chang, J. Litton, B. Arun, G. N. Hortobagyi and M. C. Hung, *Clin. Cancer Res.*, 2017, **23**, 3711–3720.
- 28 S. Wu, L. Jiang, L. Lei, C. Fu, J. Huang, Y. Hu, Y. Dong, J. Chen and Q. Zeng, *Cell Death Dis.*, 2023, **14**, 37.
- 29 S. Bilokapic, M. J. Suskiewicz, I. Ahel and M. Halic, *Nature*, 2020, **585**, 609–613.
- 30 J. H. Ding, Y. Xiao, F. Yang, X. Q. Song, Y. Xu, X. H. Ding, R. Ding, Z. M. Shao, G. H. Di and Y. Z. Jiang, *Sci. Transl. Med.*, 2024, **16**, eadg7740.
- 31 W. Jiang, Y. Li, S. Zhang, G. Kong and Z. Li, *Oncol. Lett.*, 2021, **22**, 625.
- 32 Y. Liang, H. Zhang, X. Song and Q. Yang, *Semin. Cancer Biol.*, 2020, **60**, 14–27.
- 33 M. Sixt and T. Lämmermann, *Immunity*, 2020, **52**, 721–723.
- 34 R. E. Tay, E. K. Richardson and H. C. Toh, *Cancer Gene Ther.*, 2021, **28**, 5–17.
- 35 D. S. Chen and I. Mellman, *Immunity*, 2013, **39**, 1–10.

